AAPS PharmSciTech, Vol. 10, No. 3, September 2009 (© 2009)
DOI: 10.1208/s12249-009-9250-1

Research Article

Development and Application of a Process Window for Achieving High-Quality Coating in a Fluidized Bed Coating Process

F. L. Laksmana,[1,2,5] P. J. A. Hartman Kok,[2] H. Vromans,[3,4] H. W. Frijlink,[1] and K. Van der Voort Maarschalk[1,2]

Received 22 December 2008; accepted 23 April 2009; published online 3 June 2009

Abstract. Next to the coating formulation, process conditions play important roles in determining coating quality. This study aims to develop an operational window that separates layering from agglomeration regimes and, furthermore, the one that leads to the best coating quality in a fluidized bed coater. The bed relative humidity and the droplet size of the coating aerosol were predicted using a set of engineering models. The coating quality was characterized using a quantitative image analysis method, which measures the coating thickness distribution, the total porosity, and the pore size in the coating. The layering regime can be achieved by performing the coating process at a certain excess of the viscous Stokes number (ΔSt_v). This excess is dependent on the given bed relative humidity and droplet size. The higher the bed relative humidity, the higher is the ΔSt_v required to keep the process in the layering regime. Further, it is shown that using bed relative humidity and droplet size alone is not enough to obtain constant coating quality. The changes in bed relative humidity and droplet size have been identified to correlate to the fractional area of particles sprayed per unit of time. This parameter can effectively serve as an additional parameter to be considered for a better control on the coating quality. High coating quality is shown to be achieved by performing the process close to saturation and spraying droplets small enough to obtain high spraying rate, but not too small to cause incomplete coverage of the core particles.

KEY WORDS: bed relative humidity; coating quality; droplet size; fluidized bed coating; Stokes number.

INTRODUCTION

Fluidized bed coating technology is frequently applied in the production of encapsulated products, which is of interest of many industries, such as the pharmaceutical industry. It offers the possibility to alter and to improve various characteristics of core particles such as the surface properties in a single unit operation. The challenges of using this technology are the difficulties in choosing the proper process conditions that lead to a constant coating quality and a robust process, especially during process up-scaling. One of the typical problems encountered is the occurrence of excessive core agglomeration that leads to process failure. Another problem is the occurrence of spray drying of the coating aerosol, which should also be avoided, although it is less harmful for the continuity of the process. Both cases result in poor coating quality (1,2). Therefore, it is desirable to perform coating within the layering or in the coating regime (2).

Understanding of the impact of process settings on the particle growth regimes has been the subject of many

[1] Department of Pharmaceutical Technology and Biopharmacy, University of Groningen, A. Deusinglaan 1, 9713 AV, Groningen, The Netherlands.
[2] Oral and Polymeric Product Development, Schering-Plough, PO BOX 20, 5340 BH, Oss, The Netherlands.
[3] Department of Pharmaceutics, Utrecht Institute for Pharmaceutical Sciences (UIPS), Utrecht University, PO BOX 80082, 3508TB, Utrecht, The Netherlands.
[4] Biopharmaceutics Department, Schering-Plough, PO BOX 20, 5340 BH, Oss, The Netherlands.
[5] To whom correspondence should be addressed. (e-mail: F.L. Laksmana@gmail.com)

LIST OF SYMBOLS: Cp, Specific heat capacity of dry air (kJ/kg K); C_s, Humid heat (J/g K); Cv, Specific heat capacity of water vapor (kJ/kg K); D, Mean diameter (m); F, Mass flow rate (g/s); $d_{pore,90}$, Maximum diameter of 90% number fraction of pores in a coating (μm); h, Thickness of the liquid surface layer (m); h_a, Characteristic height of surface asperities (m); h_d, Droplet height (m); k, Ratio of specific heats, Cp/Cv; M_w, Relative molecular weight (g/mol); P, Partial pressure (Pa); P_{tot}, Atmospheric pressure (Pa); Q, Volumetric flow rate (m^3/s); R, Universal gas constant (J/mol K); Re, Reynold's number; RH, Relative humidity (%); St_v, Viscous Stokes number; St_v^*, Critical Stokes number; T, Temperature (K); u, Velocity (m/s); V, Volume (m^3); X, Mass fraction; Y, Humidity; ΔSt_v, Excess in the viscous Stokes number $(St_v - St_v^*)$; λ, Specific enthalpy of evaporation (J/g); γ, Surface tension of coating solution (N/m); μ, Viscosity of coating solution (Pa s); ρ, Density (g/m^3)

SUBSCRIPTS: a, Air; ad, Adiabatic condition; atm, Atomization; bed, Particle bed; d, Droplet; d,o, Droplet at initial condition; in, At the inlet of the fluidized bed equipment; n, Nozzle/atomization; nonad, Non-adiabatic condition; orifice, Through the orifice of nozzle; out, At the outlet of the fluidized bed equipment; p, Particle/pellets/granules; s, Solution; sat, At saturation ; tip, At the tip of the nozzle; v, Water vapor; W, Water

investigations, while less works focused on their impact on coating structures. Considering the importance of both aspects on product development, this work investigates the process settings that separate layering from agglomeration regimes and from that it defines the process regime that leads to the best coating quality.

Iveson and Litster (3) proposed the distinction of various particle growth regimes inside drum granulation using the Stokes deformation number (St_{def}) and the maximum pore saturation. The application of this regime map for fluidized bed coating process is, however, not straightforward. The prediction of the granule growth regime requires information on the granule properties, i.e., granule density, yield stress, and porosity, which are not known before the process is performed. Moreover, the fluidized bed coating process involves different parameters from a mechanically agitated granulation process, which makes this regime map cannot readily be applied for the fluidized bed coating process.

In a fluidized bed process where the shear force on particles is quite low, the agglomeration tendency is rather governed by the particle coalescence than by the breakage of the granules. The successfulness of the particle coalescence depends on the availability of the liquid at the particle surface and the strength of the liquid bridge between two particles to facilitate a successful coalescence (4). To avoid particle coalescence or in other words to have a situation where colliding particles rebound, the kinetic energy upon particle collision has to exceed the viscous dissipation in the liquid and elastic losses in the solid phase (5). Ennis *et al.* (6) proposed that to be in the layering regime, the viscous Stokes number (St_v) has to be much higher than less than the critical viscous Stokes number St_v^* , defined in Eqs. 1 and 2 (5), respectively:

$$St_v = \frac{2\rho_{\mathrm{p}} d_{\mathrm{p}} u_{\mathrm{p}}}{9\mu} \tag{1}$$

$$St_v^* = \left(1 + \frac{1}{e}\right) \ln\left(\frac{h}{h_a}\right). \tag{2}$$

This model was developed by assuming elastic collisions between non-deformable particles. In practice, the particles can become deformable upon wetting by the coating liquid. The bed relative humidity and the droplet size are key parameters determining the availability of the wetting liquid on the particle surface (7–9), which then can influence the collision behavior between (wet) particles. This becomes the rationale in this study to take into account these factors together with the excess Stokes criteria in the prediction of coating regime inside the fluidized bed coater.

The bed relative humidity was predicted using mass and heat balance equations (10,11) in which the non-adiabatic situation in the coating process was considered extending the common adiabatic assumption in practice. The correlation between these process conditions and the coating quality was developed using the coating characterization results, which were obtained by performing quantitative image analysis on the images of coated particles.

THEORY

Particle Coalescence Inside a Fluidized Bed Coater

In a fluidized bed, particle velocity varies according to the variations in the particle size and particle position, leading to a variation in the Stokes number at a certain process condition. This explains the difficulty in determining the excess of Stokes number ($St_v - St_v^*$) required to be in the coating regime. In this study, we attempted to estimate this criterion.

Equations 1 and 2 were used to calculate St_{v} and St_v^* , where ρ_p, μ, d_{p}, u_{p}, e, h, h_{a} are the particle density, the viscosity of the coating solution, the (harmonic) mean diameter of two particles, the impact velocity, the coefficient of restitution, the thickness of the liquid layer at particle surface, and the characteristic height of surface asperities, respectively. The St_{v} was calculated using the maximum particle velocity and the median particle size, while the St_v^* was calculated using the maximum droplet height. In this way, the occurrence of agglomeration can be predicted, which occurs when the excess of Stokes number is below the suggested limit.

In this study, the u_{p} was taken to be the maximum particle velocity. The h was taken to be the height of the droplet (h_d), which was calculated assuming a spherical cap droplet on a flat and smooth surface. It is realized in the fluidized bed coating process that the core particles used are not flat and smooth; however, the droplet size is relatively small in comparison to the particle size used. Therefore, the curvature of the core particles can be assumed negligible. The h_{a} was calculated as the half of the difference of the maximum and the mean diameter of the granule. It is a measure of the surface roughness of the core particle. The data properties used in the calculation are presented in Table I. Relative to the particle sizes used, h_{a} is very small; therefore, the assumptions used during the calculation of droplet height are considered acceptable.

Mass and Heat Exchange in Fluidized Bed Coating Process

Fluidized bed coating process is a multiphase process where ideally the coating layer is built gradually in time. The sprayed polymer droplets hit the particles and are dried and form a coating layer as a result of their depositions on the core substrates (12). Schematically, it can be depicted as in Fig. 1. This paper focuses on the application of an aqueous coating solution. Therefore, the mass and the heat exchange during the process involves mainly the air and water components having certain conditions at the inlet (subscript *in*) and the outlet (subscript *out*) as represented in Fig. 1 (bottom). In this case, the water term also includes the moisture contained in air and the water contained in coating solution. The control volume was taken to be the volume between the air distributor and the top of the fluidized bed column. The symbols used in this paper can be found in the list of symbols.

The heat transfer in fluidized bed is known to be highly efficient. Therefore, the evaporation of water by hot air is assumed to occur instantaneously. Here, the system is assumed to be in the steady-state condition, implying that the amount of water sprayed is equal to the amount of water

Table I. Properties of Materials Used in this Study

Materials	Median Diameter (μm)	Density (kg/m^3)	h_a (μm)
Microcrystalline cellulose	275	1,463	8.5
	755	1,463	31.1
	900	1,463	32.0
Ethisphere®	328	1,518	31.9
Sanal® P	512.5	2,493	7.2
Glass beads	460	2,493	3.7
	1,000	2,531	2.9
	4,000	2,517	1.9
Suglets®	1,550	1,581	14.1
EVA	3,714	929.6	1.9
	Density (kg/m^3)	Viscosity (Pa s)	Surface tension (N/m)
HPMC E5	1,328	–	–
HPMC E5 solution	271.6224Xp+ 996.459 (16)	3.173exp(42.145Xp)/1,000 (16)	$-3.9286Xp^2+ 0.425Xp+0.45057$ (16)

EVA ethylene vinyl acetate copolymer (9% vinyl acetate) resins, *HPMC* Hydroxypropyl methylcellulose

leaving the system, as given in Eq. 3. Based on this equation, Eq. 4 can be derived:

$$\dot{F}_{\text{water,in}} = \dot{F}_{\text{water,out}} \tag{3}$$

$$Y_{\text{a,in}} \times \dot{F}_{\text{a}} + X_{\text{w}} \times \dot{F}_{\text{s}} = Y_{\text{a,out}} \times \dot{F}_{\text{a}}. \tag{4}$$

This assumption is of course not true when the amount of water sprayed exceeds the drying force of the introduced air. However, this assumption was used considering that it enables the inclusion of the over-wetting effect during the heat balance calculation, which therefore results in a correct calculation of the bed relative humidity.

The total enthalpy supplied into the fluidized bed coating system is the sum of the enthalpy of air in the inlet air, the enthalpy of moisture in the inlet air, and the enthalpy of the sprayed water, as depicted in Eq. 5. The total enthalpy leaving the system is the sum of the enthalpy of the air in the outlet air, the enthalpy of moisture in the outlet air, and the heat loss to the surroundings, as given in Eq. 6.

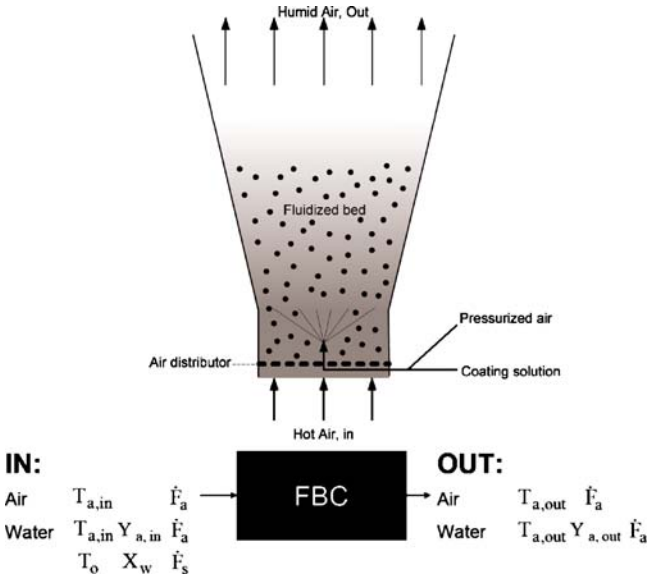

Fig. 1. Schematic representation of fluidized bed coating process

Here, room temperature (T_o) was used as temperature of reference. λ, Cp_a, and Cv_w represent specific heat of evaporation, specific heat capacity of air and water vapor, respectively.

$$\dot{Q}_{\text{total,in}} = Cp_{\text{a}}\dot{F}_{\text{a}}\left(T_{\text{a,in}} - T_{\text{o}}\right) + Cv_{\text{w}}Y_{\text{a,in}}\dot{F}_{\text{a}}\left(T_{\text{a,in}} - T_{\text{o}}\right) \tag{5}$$

$$\dot{Q}_{\text{total,out}} = Cp_{\text{a}}\dot{F}_{\text{a}}\left(T_{\text{a,out}} - T_{\text{o}}\right) + Cv_{\text{w}}Y_{\text{a,out}}\dot{F}_{\text{a}}\left(T_{\text{a,out}} - T_{\text{o}}\right) + X_{\text{w}}\dot{F}_{\text{s}}\lambda + \text{heat loss}. \tag{6}$$

Based on the steady-state assumption, the total enthalpy going out of the system is equal to the total enthalpy coming into the system. The fluidized bed system is often not fully insulated, resulting in a certain heat loss. The heat loss is dependent on the difference between the process temperature and the temperature of its surroundings. It is characterized by the heat loss coefficient (C_{heatloss}), which is normally dependent on several variables, e.g., equipment dimensions and material (13). Using these assumptions, the heat loss in Eq. 6 could be substituted with the term C_{heatloss} ($T_{\text{a,out}} - T_{\text{o}}$). Thereby, Eqs. 3, 4, 5, and 6 were solved, deriving an equation Eq. 7 which calculates the temperature of air at the outlet:

$$T_{a,out} = T_o + \frac{\left(Cp_a + Y_{a,in}Cv_w\right)\dot{F}_a\left(T_{a,in} - T_o\right) - X_w\dot{F}_s\lambda}{Cv_w\left(X_w\dot{F}_s + Y_{a,in}\dot{F}_a\right) + Cp_a\dot{F}_a + C_{heatloss}}. \tag{7}$$

MATERIAL AND METHODS

Materials

Various pellets were used as cores comprising:

1. Microcrystalline cellulose pellets 250–300, 710–800, 800–1,000 μm, which were made from Avicel PH102 FMC BioPolymer, Philadelphia, USA using the method described in (14);
2. Ethispheres® (300–355 μm), which are manufactured microcrystalline cellulose pellets, a gift from NP Pharm (Bazainville, France);

3. Sodium chloride particles, Sanal® P (425–600 μm), a gift from Akzo Nobel Salt (Amersfoort, The Netherlands);
4. Glass beads (400–520, 1,000, and 4,000 μm); and
5. EVA pellets (ATEVA® 1075A, AT Plastics Inc., Alberta, Canada), which are ethylene vinyl acetate copolymer resins containing 9% vinyl acetate.

The pellets were hand-sieved in order to obtain a specific particle size range.

Hydroxypropyl methylcellulose (HPMC; Methocel E5 LV USP/ EP premium grade, Dow) supplied by Colorcon (Dartford Kent, UK) was used as the coating material. Carmoisine (E122, Pomona BV, Hedel, The Netherlands) was used as the pigment in the coating. HPMC solution was made by dissolving HPMC polymer and carmoisine in cold water and stirring it for at least 1 h to assure the homogeneous solution.

Experimental Methods

Fluidized Bed Coating Process

The pellets were coated in a fluidized bed coater (Mycrolab, Oystar Hüttlin, Schopfheim, Germany). The HPMC solution was sprayed either from the bottom or from the top of the column. The coating process was performed until about 20% ratio of coating to core weight was sprayed. Various coating processes with different types and amounts of particle cores, different HPMC concentrations, and different process conditions were performed, which are listed in Table II.

Determination of Droplet Size

The droplet size was determined using the simplified model from Nukiyama and Tanasawa (15), which has been commonly used in practice (Eq. 8) (16):

$$d_{\mathrm{d}} = \left[\frac{585,000}{u_{\mathrm{a,tip}} - u_{\mathrm{s,tip}}}\right] \times \left[\frac{\gamma}{\rho_{\mathrm{s}}}\right]^{0.5} + 1,683\mu^{0.45}[\gamma \times \rho_{\mathrm{s}}]^{-0.225}\left[\frac{1,000}{Q_{\mathrm{a,orifice}}/Q_{\mathrm{s,tip}}}\right]^{1.5}. \quad (8)$$

Pre-calculation steps were performed to calculate the $u_{\mathrm{a,tip}}$, $u_{\mathrm{s,tip}}$, $Q_{\mathrm{a,orifice}}$, and $Q_{\mathrm{s,tip}}$ using Eqs. 9, 10, 11, 12, and 13, respectively (13). In these equations, k the ratio between Cp and Cv was taken to be 1.4 for air, while the dimensions of the nozzle, d_{n} and d_{orifice}, were 0.6 and 1.2 mm, respectively. The HPMC solution properties used for the calculation are given in Table I.

$$u_{\mathrm{a,tip}} = \sqrt{\frac{2kRT_0}{(k+1)Mw_{\mathrm{a}}}} \quad (9)$$

$$u_{\mathrm{s,tip}} = \frac{\dot{F}_{\mathrm{s}}}{0.25\pi d_{\mathrm{n}}^2 \rho_s} \quad (10)$$

$$\rho_{\mathrm{a,cr}} = \left(\frac{2}{k+1}\right)^{1/(k-1)} \rho_a(T_0) \quad (11)$$

$$Q_{\mathrm{a,orifice}} = \frac{P_{\mathrm{n}} A_{\mathrm{orifice}} \sqrt{\left(\frac{2}{k+1}\right)^{(k+1)/(k-1)} \left(\frac{k\,\mathrm{Mw}_a}{RT_0}\right)}}{\rho_{\mathrm{a,cr}}} \quad (12)$$

$$Q_{\mathrm{s,tip}} = \frac{\dot{F}_{\mathrm{s}}}{\rho_{\mathrm{s}}}. \quad (13)$$

In this study, the initial droplet size was varied by changing the atomization pressure between 0.5 and 1.5 bar and the concentration of the HPMC solution from 5% to 10%. The droplet sizes obtained vary between 33 and 364 μm.

Determination of Particle Impact Velocity

The particles inside the fluidized bed equipment were tracked using a high-speed camera Motion Xtra HG-100K, Redlake, Tallahassee, USA. The camera was placed in front of the monitor glass, which is a few centimeters above the air distributor. The images were recorded at a speed of 3,000 frames per second, which enables the determination of the particle velocity in the range studied. The obtained images are 736×768 pixels in size and have a pixel size of 12.98×13.33 μm^2.

The particle velocity was determined by tracking the particle displacement over time, which was performed using Motion Pro Studio™ software IDT Vision, Lommel, Belgium. The particle velocity was determined as the maximum velocity of 15–20 particles, which were tracked for each test performed.

Particle velocities of various particle sizes at different fluidizing air velocities were measured, from which data correlation for particle velocity was developed. The model used is similar to that of Kunii and Levenspiel (17). Some of the parameters had to be derived empirically due to the differences in the air distributor and the design of the fluidized bed column used in this study. The obtained correlations are shown in Table III.

Determination of the Agglomeration Occurrence

The occurrence of agglomeration was monitored by measuring the particle size before and after the coating process. The agglomeration was signified when the size of more than 10% weight fraction of the particles is larger than the cutoff diameter. The cutoff diameter was determined by calculating the maximum size of coated pellets obtained after the coating process if the coating film was formed by layering. This criterion differs for the core particles used, as listed in Table IV.

Characterization of the Coating

The coating structures were analyzed using a quantitative image analysis method described previously (14). The analysis comprised the characterization of coating thickness distribution, the porosity, and the pore size distribution in the coating. The results were represented as the qualities critical to the coating functionalities, which are the minimum coating

Table II. Experimental Program Used in this Study

No.	Core type (μm)	Spraying direction	Bed mass (g)	X_{HPMC} (%)	Q_{fa} (m^3/h)	P_{atm} (bar)	$\dot{F}_s$ (g/min)	$T_{a,in}$ (K)	$T_{a,out}$ (K)
1	MCC 800–1,000	BS	150	5	25	1.5	6.6	343.2	301.7
2						1.5	5.0	343.2	306.8
3						1.5	2.4	343.2	313.8
4						0.5	2.4	343.2	314.1
5						1.5	2.4	333.2	308.7
6						1.5	4.8	323.2	296.4
7						1.5	2.4	323.2	302.8
8						1.5	2.4	313.2	296.7
9						1	2.4	313.2	297.2
10						0.5	2.4	313.2	297.2
11		TS				0.5	4.8	343.2	309.2
12	Salt 425–600	BS	150	5	25	1.5	3.0	333.2	305.0
13					20	1.5	3.0	333.2	301.2
14					20	1.5	3.0	313.2	294.6
15	ES 300–355	BS	150	5	25	1.5	3.6	343.2	312.2
16	GB 400–520	BS	150	5	25	1.5	3.0	333.2	307.0
17	GB 4,000		50			1.5	1.2	333.2	310.5
18						1	1.2	333.2	313.5
19						0.5	1.2	323.2	308.2
20						0.5	1.2	313.2	302.7
21	MCC 800–1,000	BS	150	5	15	1.5	2.4	343.2	291.7
22					25	1.5	5.0	353.4	314.1
23						1.5	4.0	353.9	315.7
24						1.5	4.8	313.2	294.3
25						1.5	4.8	343.2	305.4
26						1	4.8	343.2	307.5
27						0.5	4.8	343.2	307.6
28						1	2.4	343.2	313.7
29	MCC 250–300					1.5	4.2	333.2	303.2
30	MCC 710–800					1	3.0	333.2	307.2
31	MCC 800–1,000			10		0.5	4.2	343.1	310.9
32						0.5	3.0	343.1	312.7
33		TS		5		1.5	4.8	343.1	305.9
34	EVA 3600–3,800	BS	50	5	25	1.5	2.8	343.1	313.2
35						1.5	1.4	343.1	315.8
36						1.5	1.4	313.2	300.0
37	GB 4,000	BS	50	5	20	1.5	2.4	333.2	310.5
38					25	0.5	1.2	333.1	313.3
39	GB 1,000	BS	60	5	25	0.5	5.8	333.2	307.8
40	Suglets 1,400–1,700	BS	50	5	25	1.5	3.0	343.2	311.9
41						1.5	1.2	343.1	316.2
42						1.5	1.2	343.1	315.3

MCC microcrystalline cellulose pellets, *ES* Ethispheres®, *GB* glass beads, *EVA* ethylene vinyl acetate copolymer (9% vinyl acetate) resins, *BS* bottom spray, *TS* top spray

thickness, the span of the coating distribution $\frac{\Delta x_{90}-\Delta x_{10}}{\Delta x_{50}}$, the total porosity, and the size of the largest pores ($d_{pore,90}$).

RESULTS AND DISCUSSION

Prediction of Bed Relative Humidity

Different fluidized bed coating processes using various cores and process conditions were performed, resulting in different air temperatures at the outlet ($T_{a,out}$) which were measured, and their data are given in Table II. These data were split into two sets: one was used to obtain the heat loss coefficient and the other one was used to test the model.

Table III. Correlation for the Particle Velocity (U_p) and its Constants as a Function of the Particle Size (d_p), Particle Density (ρ_p), and Inlet Air Velocity (U_{fa})

$$U_p = b_1 \rho_p d_p^{-b_2} \left(U_{fa} - b_3 \rho_p d_p^{b_4}\right)^{b_5}$$

Constants	Values
b_1	10.673
b_2	0.279
b_3	2.764×10^{-5}
b_4	1.233
b_5	1.037
R^2	0.974

Table IV. Cutoff Coated Pellet Diameter to Determine the Occurrence of Agglomeration in Experiments

Core particles (μm)	Cutoff diameter (μm)
MCC 250–300	315
MCC 710–800	830
MCC 800–1,000	1040
ES 300–350	365
Salt 425–600	640
GB 400–520	550
GB 1,000	1,070
GB 4,000	4,250
EVA	3,940

MCC microcrystalline cellulose pellets, *ES* Ethispheres®, *GB* glass beads, *EVA* ethylene vinyl acetate copolymer (9% vinyl acetate) resins

The data from the first set, which are from the experiment nos. 1 to 20, were fitted to Eq. 7. Using 'fminsearch' command in MATLAB™, different values of $C_{heatloss}$ were automatically tested into the model until the differences between the calculated and the measured values of the air temperature at the outlet are minimized. The best value for $C_{heatloss}$ was found to be $6.1287 \pm 0.637 \times 10^{-3}$ J/K.

Furthermore, the model was validated using the air temperature at the outlet measured from experiment nos. 21 to 42. These measured values were compared with the predicted air temperature at the outlet using the present heat and mass balance model (Eq. 7). The results shown in Fig. 2 verify that our model predicts the air temperature at the outlet quite well, with a degree of fit of 0.99.

No significant effects were found of core properties (type and diameter) and droplet properties (atomization pressure) on the prediction quality of the model. The fact that the outlet air temperature can be well predicted by considering only the total fluidized bed system without looking at the core and droplet properties confirms the highly efficient energy transfer between the drying air and the coating solution assumed in the model.

Having determined the air temperature, the humidity of the air at the outlet enables the calculation of the bed relative humidity following the method described in the Appendix. The same value of RH_{bed} can be obtained from different combinations of spraying rate, inlet air temperature, and flow rate. This suggests the suitability of using this process parameter to simplify the amount of process parameters to be evaluated for example during up-scaling.

Determination of Coating Process Regime

As discussed earlier in "THEORY," the agglomeration tendency during the fluidized bed coating process is determined by the availability of liquid on the surface of the particle and the liquid strength to keep the particles together until solid bridges between the particles are formed. Intuitively, the amount of liquid on the particle surface can be minimized by fast drying or slow spraying. This condition is related to low bed relative humidity. Furthermore, using a small droplet size also enables fast drying, which will limit the number of successful particle coalescences. Therefore, both the bed relative humidity (RH_{bed}) and the relative (initial) droplet size to core size ($d_{droplet,o}/d_{core}$) were applied together with the excess of viscous Stokes number (ΔSt_v) criteria proposed by Ennis *et al.* (6) to develop the regime criteria in the fluidized bed coating process.

Amongst the experiments performed in this study, agglomeration occurred during experiment nos. 1, 6, 11, 14, 27, 29, 31, and 32. In these experiments, more than 10% of the pellets were agglomerated. The bed collapsed after the process started in experiment nos. 21, 24, and 39. These 11 experiments are classified to be in the agglomeration regime. The rest of the experiments were presumed to occur in the layering regime.

Figure 3 shows the ΔSt_v, RH_{bed}, and $d_{droplet,o}/d_{core}$ conditions for each experiment where the layering and agglomeration regimes were indicated in the figure labels. It is shown in this figure that the two regimes were separated by certain combinations of the ΔSt_v, RH_{bed}, and $d_{droplet,o}/d_{core}$. The transition points were taken from the conditions which are in the middle of the conditions of experiments under layering condition which is close to the granulation condition and vice versa. The corresponding ΔSt_v, RH_{bed}, and $d_{droplet,o}/d_{core}$ at the transition points were then fitted to the partial least-square model, resulting in Eq. 14 with degree of fit (R^2) of 0.95.

$$\Delta St_v = 1207 RH_{bed} + 301 \ \ d_{droplet}/d_{core} - 990. \qquad (14)$$

This equation forms a surface plot that separates the layering and agglomeration regimes shown in Fig. 3. This plot shows that certain excess of viscous Stokes number is required to keep the process in the layering regime at a given bed relative humidity and relative droplet size. The inserted plot in Fig. 3 is meant to illustrate better the correlation between these three variables. The different colors in the image represent the different minimum values of the ΔSt_v required to be in a layering regime at various bed relative humidities and relative droplet size.

At a lower RH (e.g., at 70%), the ΔSt_v is shown to vary between 0 and about 40 (shown as dark and lighter blue colors, respectively) at a whole range of relative droplet sizes tested (10–60%; see the inserted plot in Fig. 3). With increasing RH, the variation in ΔSt_v becomes bigger with increasing relative droplet size (e.g., varying from 250 to 400 when relative droplet size changes from 10% to 60% at 100% RH). The higher the bed relative humidity and the relative droplet size, the higher is

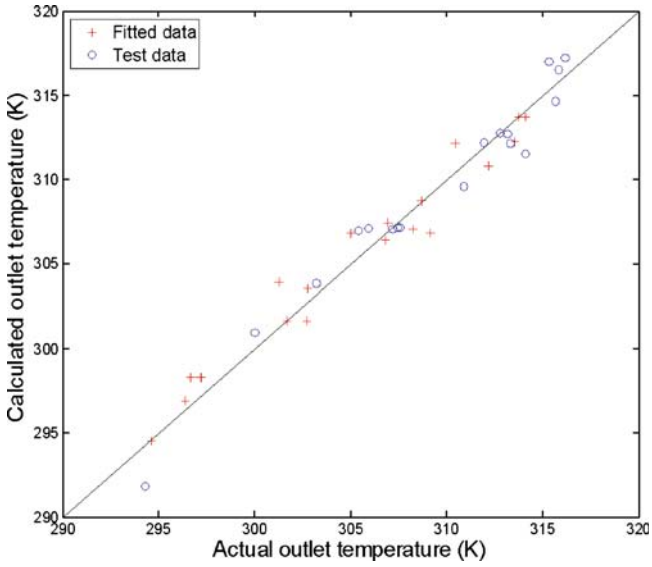

Fig. 2. Verification of the model to predict the air temperature at outlet

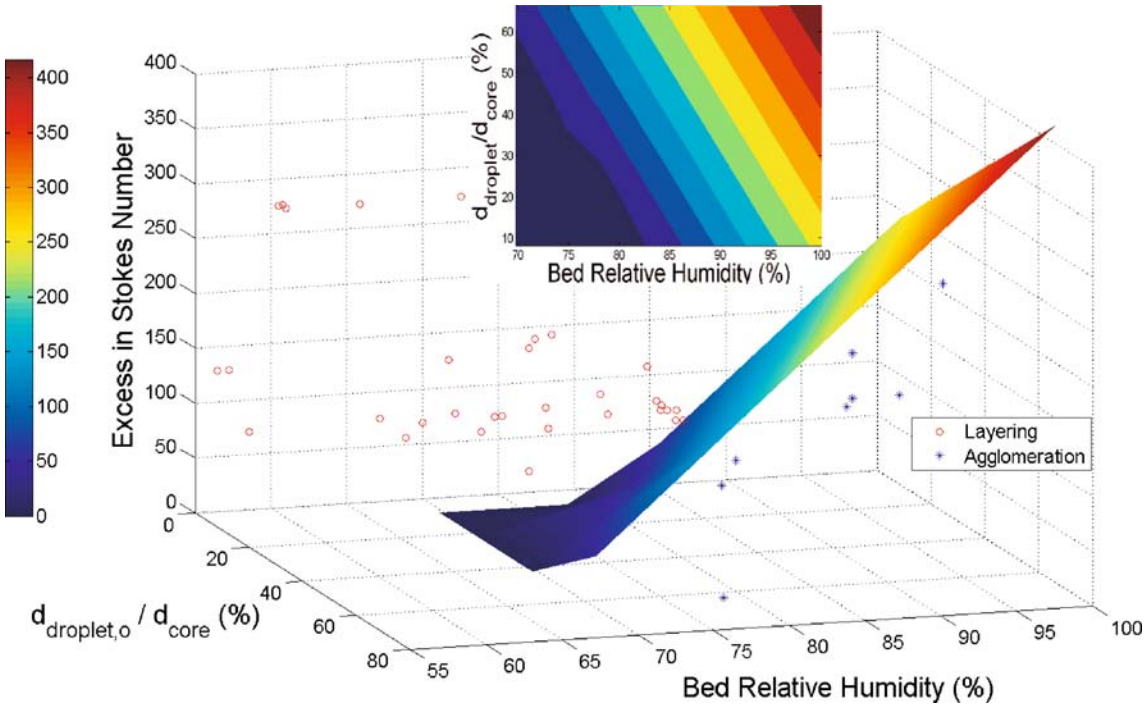

Fig. 3. Process regime map determined by the combination of ΔSt_v, RH_{bed}, and $d_{droplet,o}/d_{core}$ in the fluidized bed coater

the ΔSt_v required. Knowing the required ΔSt_v enables the process settings to be adjusted accordingly by changing, i.e., the particle velocity, the particle size, and density and the viscosity of the coating solution. The ability to predict the occurrence of agglomeration helps to design the experimental program more effectively by selecting only those process settings that lead to the layering regime.

Process Adjustment and Its Effect on Coating Quality

Having determined the process windows for performing the coating process in the layering regime leads to the next step, i.e., finding the optimum process conditions, which lead to the best coating quality. Coating quality can be described in terms of the uniformity of the coating thickness and the porosity of the coating. The uniformity in coating thickness can be quantified by the minimum coating thickness and the span of the coating thickness distribution. A very low minimum coating thickness is not desirable, as it indicates the incomplete or poor coverage of the core particles. A wide span of the coating thickness distribution is either unwanted, as it will lead to a big variation in the coating transport properties, which are particularly important for coating applied for controlled/extended release purposes.

The effects of the process conditions focusing on properties that describe the coating quality were further assessed. The results shown were taken from the experiments (of which conditions are listed in Table II) using the microcrystalline cellulose pellets (800–1,000 μm) as core particles.

Figure 4 shows the effect of increasing bed relative humidity (in this case by reducing the inlet air temperature) on the coating thickness distribution. It is shown that a maximum in the minimum coating thickness and a minimum span of coating thickness distribution were achieved when the coating process was performed at a high relative humidity of the bed. Figure 5 shows another positive effect of increasing the bed relative humidity on coating quality where the coating porosity and the pore size are reduced. At high relative humidity, there is less chance for premature drying of the coating droplets. Consequently, the coating droplets are still wet upon collision with particles, enabling the droplet to spread well on particle, which results in a more homogeneous and less-porous coating structure.

A discontinuity in the correlation between the bed relative humidity and the coating quality is noticed in Figs. 4 and 5 between processes performed using spraying rates of 2.4 and 4.8 g/min. At these different spraying rates, both the relative initial droplet size and the spraying flux rate (defined as the fractional area of particles sprayed per unit of time) are changed.

The interdependency between process parameters in the fluidized bed coating process has been identified. The inlet air temperature and the spraying rate together influence the relative humidity. Either the changes in the atomization pressure or in the spraying rate vary the (relative) initial droplet size. Together with the spraying rate, the respective droplet size will determine spraying flux rate. Consequently, it was difficult to vary one condition without changing other conditions and keeping the process in the layering regime at the same time.

Figure 6 illustrates the interrelationship between these process settings and the range of the process parameters varied in this study, which is limited to the process settings that avoid the occurrence of agglomeration. This figure shows for example that the bed relative humidity can be varied extensively without causing any agglomeration, and any significant changes in the spraying flux rate when the droplets sprayed are small enough. Moreover, this figure supports the discussion on the selection of the process settings for achieving the best coating quality based on Figs. 7 and 8.

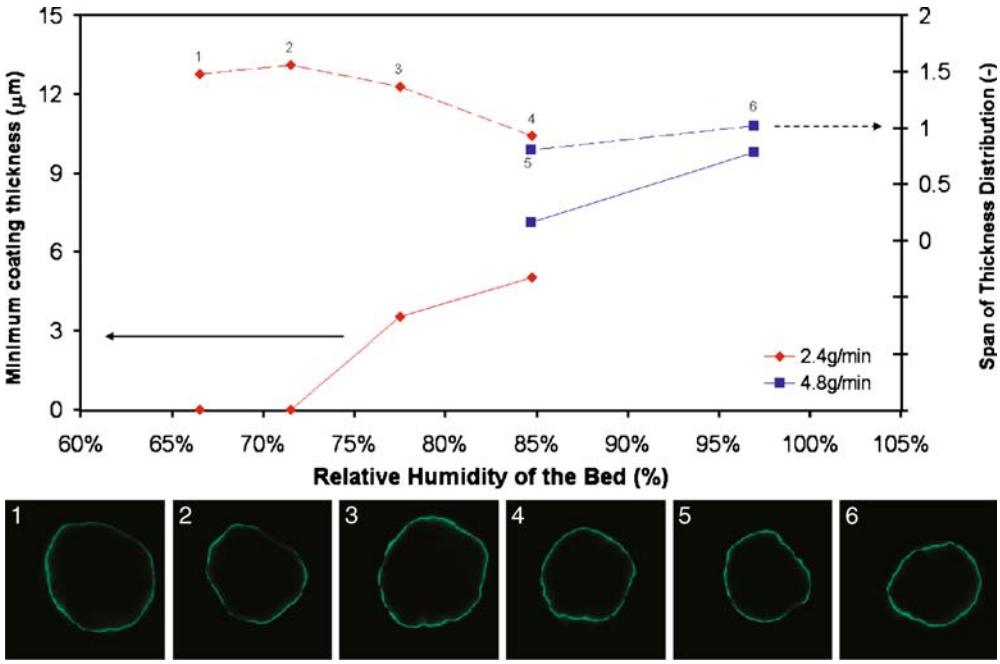

Fig. 4. Effect of bed relative humidity on the minimum coating thickness and the span of the coating thickness distribution. *Underneath the plot* are the CSLM images of coated particles with corresponding numbering as in the data plots

Figures 7 and 8 were plotted to illustrate the combined effect of these process conditions on minimum coating thickness and coating porosity, respectively. These plots were made by making a data grid from the experimental data using a "v4" method in MATLAB™.

High coating quality implies the absence of areas with only a thin thickness, meaning that the minimum coating thickness is close to the average thickness. The average coating thickness obtained in this study is between 25 and 30 μm. Figure 7 shows that the minimum of coating thickness is closest to the average thickness at bed relative humidity close to saturation and at droplet size around 10% to 30% of particle size, which corresponds to high spraying flux rate ($\sim 7–10\times10^{-3}$ s^{-1}). A high spraying flux rate implies a high probability for droplets to cover the particle surface. The relative droplet size indicates the fraction of particle covered by a droplet every time it reaches the particle. The actual coverage of particle by droplets can therefore be estimated

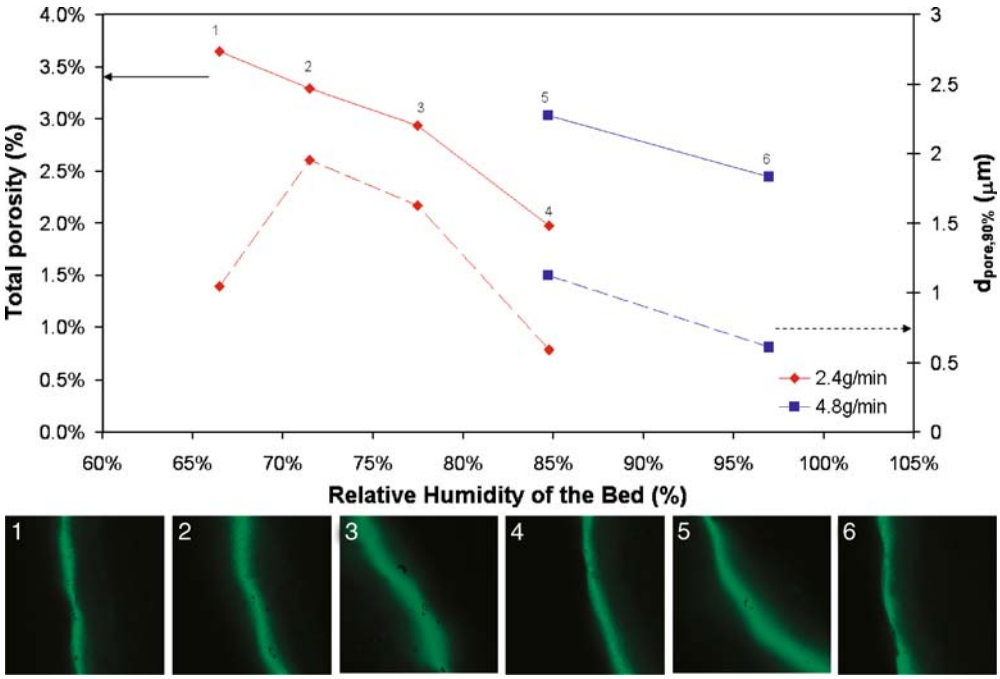

Fig. 5. Effect of bed relative humidity on coating porosity and pore size. *Underneath the plot* are the CSLM images of coating layer on particles with corresponding numbering as in the data plots

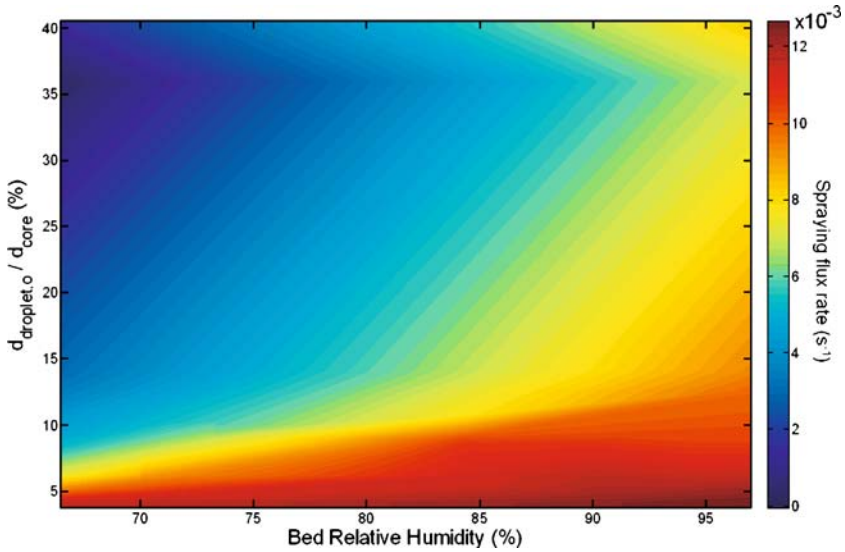

Fig. 6. The combination of the process settings used in this study between the relative droplet size, bed relative humidity and spraying flux rate (defined as the fractional area of particle sprayed per unit time)

from the product between the probability (the spraying flux rate) and the droplet size relative to the particle size. When these factors are higher, the coating coverage on the core particles becomes better. This explains why at low relative droplet size (below 5%), the minimum coating thickness is low, although the spraying flux rate is high. A similar reason exists for the coating process using high relative droplet size (above 30%) where the spraying flux rate is low and therefore the minimum coating thickness obtained is low.

Figure 8 shows similar effects of the combination between the relative humidity, the relative droplet size, and the spraying flux rate on coating porosity. Minimum coating porosity is desired. This can be obtained by performing the coating process at a bed relative humidity close to saturation. At this point, the variations in the relative droplet size as well as in the spraying flux rate do not influence the coating porosity. Close to saturation, droplets evaporate slowly, which facilitates enough time for the coating solution to rewet the precursor film and fill in the existing pores, resulting to a dense coating. Porous coating is obtained at low bed relative humidity at high relative droplet size. This condition corresponds to a low spraying flux rate. This result shows the severe impact of the combination between fast drying and low distribution of droplets on coating porosity obtained.

CONCLUSIONS

In this study, the relation between the excess in viscous Stokes number and the bed relative humidity and droplet size has been developed. These criteria have been used to determine the process regime inside a fluidized bed coater that leads to the best quality of the coating. The ability to estimate the coating regime will help the design of a more efficient experimental program in development.

The interdependency between the bed relative humidity, droplet size, and the fractional area of particle sprayed per

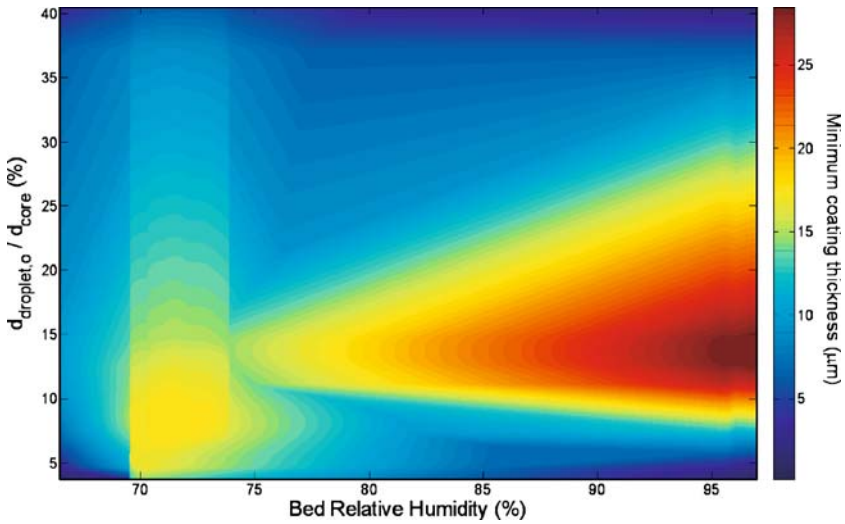

Fig. 7. Contour plot of the effect of the relative initial droplet size and the bed relative humidity on the minimum coating thickness

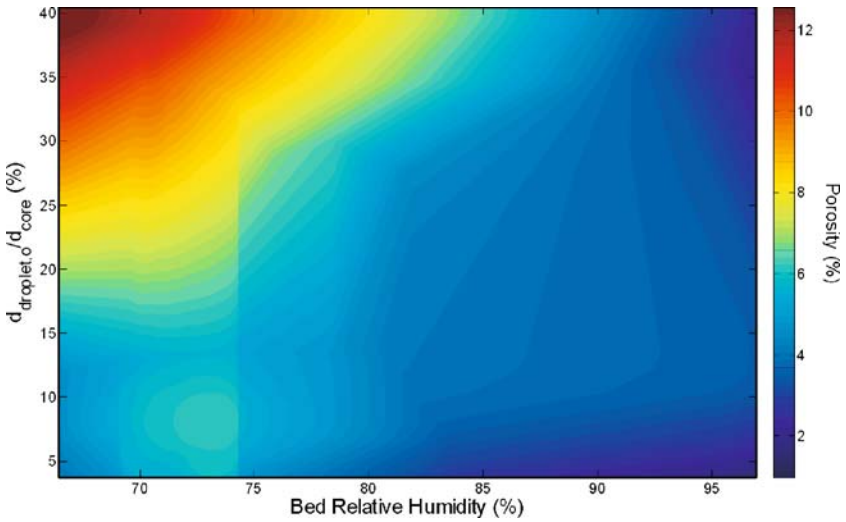

Fig. 8. Contour plot of the effect of the relative initial droplet size and the bed relative humidity on the coating porosity

unit of time (spraying flux rate) has been identified. They are shown to be important in controlling coating quality, whose influences have to be assessed at once. High coating quality defined as having a uniform coating (minimum coating thickness close to mean coating thickness) and low porosity can be achieved by performing the coating process close to saturation. Using a small droplet size leads to a high spraying rate that is required for obtaining high coating quality. Nevertheless, the droplet size should not be too low, since that may cause incomplete coverage of core particles.

ACKNOWLEDGMENTS

The authors would like to thank Mario Campana for his contribution on the derivation of the correlations for the hydrodynamic properties of the fluidized bed coater used for our study. We would also like to thank Friesland Food Research Centre Deventer, The Netherlands, especially Drs. Marcel Paques for letting us use their CSLM facility and Ing. Anno Koning for performing the CLSM measurements.

APPENDIX

The drying path by air inside a fluidized bed coating process is schematically given in Fig. 9. In this figure, the adiabatic saturation line is represented by the *blue solid line*. When there is heat loss, the drying process in the fluidized bed coater no longer follows the adiabatic saturation line but a path, which typically follows the *red solid line* as represented in this figure. Under this condition, the maximum amount of water vapor that the drying air can contain before it becomes saturated ($Y_{\text{a,sat-nonad}}$) is lower than that in the adiabatic process ($Y_{\text{a,sat-ad}}$). In this study, the ($Y_{\text{a,sat-nonad}}$) was estimated using a hypothetical adiabatic saturation line. Due to heat loss, the air temperature at the outlet ($T_{\text{a,out}}$) is also lower than that in the adiabatic process $T^*_{a,out}$. A hypothetical adiabatic saturation line was drawn, which passes the actual air temperature at the outlet ($T_{\text{a,out}}$), shown as a *blue dashed line* in Fig. 9. This line starts at an inlet air temperature ($T^*_{a,in}$) lower than the actual inlet air temperature ($T_{\text{a,in}}$). Working in the same range of air humidities at the inlet and the outlet in both adiabatic and non-adiabatic processes, the difference between the $T_{\text{a,in}}$ and the $T^*_{a,in}$ is equal to the difference between the outlet air temperature in adiabatic $T^*_{a,out}$ and non-adiabatic ($T_{\text{a,out}}$) conditions, as depicted in Eq. 15. The $T^*_{a,out}$ was calculated using Eq. 5 by neglecting the term C_{heatloss}.

$$T^*_{a,\text{in}} = T_{\text{a,in}} - (T^*_{\text{a,out}} - T_{\text{a,out}}). \tag{15}$$

Graphically, the actual saturated humidity of air ($Y_{\text{a,sat-nonad}}$) could be determined by following the hypothetical adiabatic saturation line using a psychrometry chart. To enable automatic calculations using a computer, in this study, it was calculated using the following equations:

• Equation 16 describes the correlation between the saturation water vapor pressure and temperature, which is valid for the temperature range between 25°C and 100°C (13).

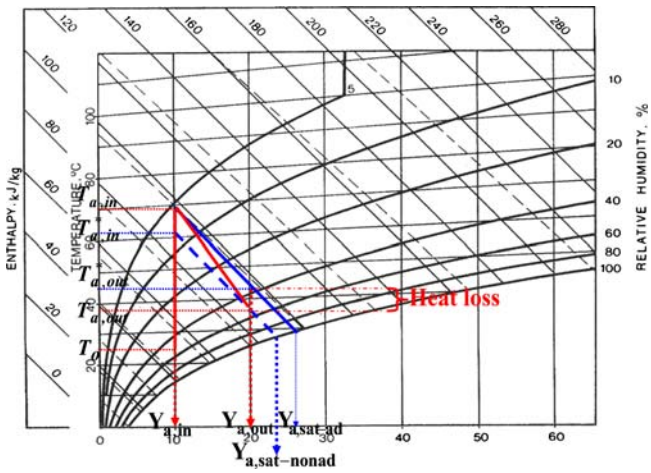

Fig. 9. Schematic diagram of enthalpy, temperature, and humidity changes during fluidized bed coating process. *Blue line* represents the adiabatic saturation process, while *red line* represents the non-adiabatic drying path in the actual process

• Substituting this relation to Eq. 17, the air temperature at saturation point could be calculated. For water–air mixture, $\frac{c_s}{\lambda}$ is equal to 4.45×10^{-4} (13).

• Further on, the saturated humidity of air ($Y_{\text{a,sat-nonad}}$) was calculated using Eq. 18. Finally, the bed relative humidity (RH_{bed}) was calculated using Eq. 19.

$$P_{\text{sat}} = 2.740938 \times 10^{-37}\left(T_{\text{a,sat}}\right)^{16.19334} \tag{16}$$

$$T_{\text{a,sat}} = T^{*}_{\text{a,in}} + \frac{Y_{\text{a,in}} - \frac{P_{\text{sat}}}{P_{\text{tot}}-P_{\text{sat}}} \times \frac{\text{Mw}_{\text{w}}}{\text{Mw}_{\text{a}}}}{c_{\text{s}}/\lambda} \tag{17}$$

$$Y_{\text{a,sat-nonad}} = \frac{P_{\text{sat}}}{P_{\text{tot}} - P_{\text{sat}}} \times \frac{\text{Mw}_{\text{w}}}{\text{Mw}_{\text{a}}} \tag{18}$$

$$\text{RH}_{\text{bed}} = \frac{Y_{\text{a,out}}}{Y_{\text{a,sat-nonad}}} \times \frac{\text{Mw}_{\text{w}}/\text{Mw}_{\text{a}} + Y_{\text{a,sat-nonad}}}{\text{Mw}_{\text{w}}/\text{Mw}_{\text{a}} + Y_{\text{a,out}}}. \tag{19}$$

REFERENCES

1. Takei N, Unosawa K, Matsumoto S. Effect of the spray-drying process on the properties of coated films in fluidized bed granular coaters. Adv Powder Technol 2002;13:333–42.
2. Hede PD, Bach P, Jensen AD. Small-scale top spray fluidized bed coating: Granule impact strength, agglomeration tendency and coating layer morphology. Powder Technol 2007;176:156–67.
3. Iveson SM, Litster JD. Growth regime map for liquid-bound granules. AIChE J 1998;44:1510–18.
4. Liu LX, Litster JD, Iveson SM, Ennis BJ. Coalescence of deformable granules in wet granulation processes. AIChE J 2000;46:529–39.
5. Iveson SM, Litster JD, Hapgood K, Ennis BJ. Nucleation, growth and breakage phenomena in agitated wet granulation processes: a review. Powder Technol 2001;117:3–39.
6. Ennis BJ, Li J, Tardos GI, Pfeffer R. A microlevel-based characterization of granulation phenomena. Powder Technol 1991;65:257–72.
7. Tang ESK, Wang L, Liew CV, Chan LW, Heng PWS. Drying efficiency and particle movement in coating-impact particle agglomeration and yield. Int J Pharm 2008;350:172–80.
8. Hede PD, Bach P, Jensen AD. Top-spray fluid bed coating: scale-up in terms of relative droplet size and drying force. Powder Technol 2008;184:318–32.
9. Liu LX, Litster JD. Spouted bed seed coating: the effect of process variables on maximum coating rate and elutriation. Powder Technol 1993;74:215–30.
10. Tanya am Ende M, Berchielli A. A thermodynamic model for organic and aqueous tablet film coating. Pharm Dev Technol 2005;10:47–58.
11. Larsen CC, Sonnergaard J, Bertelsen P, Holm P. A new process control strategy for aqueous film coating of pellets in fluidized bed. Eur J Pharm Sci 2003;20:273–83.
12. Saleh K, Cherif R, Hemati M. An experimental study of fluidized-bed coating: influence of operating conditions on growth rate and mechanism. Adv Powder Technol 1999;10:255–77.
13. Perry RH, Green DW. Perry's chemical engineers' handbook. New York: McGraw-Hill; 1997.
14. Laksmana FL, Van Vliet LJ, Hartman Kok PJA, Vromans H, Frijlink HF, Van der Voort Maarschalk K. Quantitative image analysis for evaluating the coating thickness and pore distribution in coated small particles. Pharm Res 2009;26:965–76. doi:10.1007/s1.1095-008-9805-y.
15. Nukiyama S, Tanasawa Y. Experiments on the atomization of liquids in an air stream. Trans Soc Mech Eng Japan 1939;5:68–75.
16. Cole G, Hogan J, Aulton M. Pharmaceutical coating technology. London: Taylor and Francis; 1995.
17. Kunii D, Levenspiel O. Fludization engineering. Melbourne: Krieger; 1977.